Water Supply

Water Supply Vol 22 No 3, 2896 doi: 10.2166/ws.2021.429

Removal of As(V) from aqueous solutions using calcium-alginate microspheres with encapsulated iron nanoparticles

María Soledad Ruiz-Mora[a], Ruth Alfaro-Cuevas-Villanueva[b], Verónica Martínez-Miranda[c], Orlando Hernández-Cristóbal[d] and Raúl Cortés-Martínez[e,*]

[a] Maestría en Ciencias en Ingeniería Ambiental, Facultad de Ingeniería Química, Universidad Michoacana de San Nicolás de Hidalgo. CP 58030. C.U., Morelia, Michoacán, México
[b] Instituto de Investigaciones en Ciencias de la Tierra, Universidad Michoacana de San Nicolás de Hidalgo. C.U., CP 58030, Morelia, Michoacán, México
[c] Instituto Interamericano de Tecnología y Ciencias del Agua, Facultad de Ingeniería, Universidad Autónoma del Estado de México, Toluca, México
[d] Escuela Nacional de Estudios Superiores (ENES), Unidad Morelia, UNAM, Antigua Carretera a Pátzcuaro 8701, col. Ex Hacienda San José de la Huerta, Morelia, Michoacán, México
[e] Facultad de Químico Farmacobiología, Universidad Michoacana de San Nicolás de Hidalgo, Tzintzuntzan 173 Col. Matamoros, CP 58240, Morelia, Michoacán, México
*Corresponding author. E-mail: raulcortesmtz@gmail.com

RA-C-V, 0000-0002-5666-0695; OH-C, 0000-0001-5460-0536; RC-M, 0000-0001-8990-2403

ABSTRACT

This work investigated As(V) removal from aqueous solutions using calcium alginate microspheres with encapsulated iron nanoparticles (FeNPs) in batch systems. The kinetic, equilibrium, and thermodynamic parameters of the adsorption process were evaluated. Adsorbents were characterized using Fourier Transform Infrared Spectroscopy, Scanning Electron Microscopy, and Zeta Potential techniques. The FeNPs were obtained by a simple and low-cost method and they were successfully encapsulated and uniformly dispersed over the microspheres' surface. Significantly fast adsorption kinetic rates were observed due to microspheres' particle size and FeNPs encapsulation. The chemisorption mechanism was recognized in both adsorbate-adsorbent systems. The As(V) isotherms data suggested that the process is associated with heterogeneous adsorption. Available sorption sites with different adsorption energies were related to the functional groups involved in removing As(V), such as hydroxyl and carboxyl groups. Significantly high adsorption capacities were obtained for both materials, suggesting they can be competitive compared to conventional adsorbents, even at low FeNPs concentrations. Besides FeNPs encapsulation enhancing arsenate removal, higher adsorption was obtained at slightly acidic pH values and, together with their small particle size, suggests that the microspheres have a great potential to be used as arsenate adsorbents in the water treatment for human consumption.

Key words: adsorption, Alginate, arsenic, iron nanoparticles, microspheres

HIGHLIGHTS

- Iron nanoparticles were successfully prepared and encapsulated using simple methods.
- Iron-modified alginate microspheres were highly effective for As(V) removal, particularly at low concentrations.
- Fast removal was observed for both arsenate-adsorbent systems.
- Significantly high adsorption capacities were obtained for both adsorbents, using low iron nanoparticles concentrations in the microspheres.

ABBREVIATIONS

AAS	Atomic absorption spectroscopy
ACs	Activated carbons
Alg-As	Arsenic-loaded alginate microspheres
AlgFe	Alginate microspheres with encapsulated iron nanoparticles
AlgFeAs	Arsenic-loaded alginate microspheres with encapsulated iron nanoparticles
AlgN	Calcium alginate microspheres

D-R	Dubinin-Radushkevich model
EDS	Energy Dispersive X-Ray Spectroscopy
FeNPs	Iron nanoparticles
FTIR	Fourier Transform Infrared Spectroscopy
δ	Zeta Potential
LF	Langmuir-Freundlich model
pH_{PZC}	Point of Zero Charge
SEM	Scanning Electron Microscopy
$\Delta G°$	Gibbs free energy
$\Delta H°$	Change in enthalpy
$\Delta S°$	Change in entropy

INTRODUCTION

Arsenic is a natural element present in the earth's crust that can appear in water through processes of chemical weathering or dissolution of minerals, or anthropogenic pollution due to mining activity, use of pesticides, use of fossil fuels, and the treatment of wood (Sarkar *et al.* 2006; Wang *et al.* 2020). Hence, the World Health Organization (WHO), in agreement with the U.S. Environmental Protection Agency (US-EPA), recommended 0.01 mg/L as an arsenic concentration limit for drinking water (Maity *et al.* 2021). However, in some countries, like Mexico, the regulations are more flexible, and the permissible arsenic level for drinking water has been set at 0.025 mg/L (Burillo *et al.* 2021).

Through ingestion, continuous exposure to arsenic can cause several dysfunctions and diseases such as loss of appetite and nausea, muscle weakness, and gastrointestinal symptoms (Mandal *et al.* 2013). However, people who consume water with amounts greater than 0.05 mg/L of this metalloid have shown lesions such as hyperkeratosis, changes in pigmentation, various types of cancer, like skin, lung, kidney, liver, and bladder (Habuda-Stanić & Nujić 2015; Palma-Lara *et al.* 2020). The chemistry of this element includes the existence of different oxidation states, with the species As(III) and As(V) being the most commonly found in natural waters, depending on their pH value (Sousa *et al.* 2015). Arsenite is more toxic and mobile than arsenate, but arsenate in contaminated groundwater is more common, particularly in shallow aquifers. Even though natural sources are the primary source of exposure to arsenic through water, it has been reported in some countries that industrial activities can also represent a high risk of exposure, even at higher concentrations of this element (Boffetta *et al.* 2020).

In addition, the problem of a sufficient and high-quality water supply for human consumption is increasing worldwide. Many countries confront situations where a groundwater source has to be used because of the scarcity of surface water bodies, so it is necessary to exploit aquifers with high levels of arsenic (Kumar *et al.* 2020). Moreover, it is estimated that approximately 140 million inhabitants in almost 70 countries may be exposed to this metalloid through contaminated water; particularly in Latin America, nearly 14 million people are at potential risk of arsenic exposure (Kumar *et al.* 2020; Osuna-Martínez *et al.* 2021). Therefore, it is necessary and imperative to investigate and generate new arsenic removal technologies for this type of polluted water, or even modify and optimize the existing ones, so that they can be highly efficient and easy to implement, especially in developing countries, where water treatment costs could be a major limiting factor.

Different treatment methods for removing arsenic from water include coagulation-flocculation, precipitation, and membrane processes (Nazari & Halladj 2014; Wang *et al.* 2015). However, these methods are generally expensive, involve maintenance, monitoring systems, high reagent consumption or energy requirements, and generation of toxic sludge or other waste products that require elimination and subsequent treatment (Xi & Chen 2014). Thus, it is necessary to find consistent and straightforward technologies that use local resources to remove this element from groundwater used for human consumption at a relatively low cost (Kumar *et al.* 2019). Among these treatment methods, adsorption has been one of the most studied technologies for removing arsenic from water for human consumption in recent years. It is an effective and efficient method, particularly at low pollutant concentrations, and is relatively simple to implement and operate. In addition, the use of low-cost adsorbents with high removal efficiency makes adsorption a cost-effective process that does not require high energy consumption, does not produce toxic effluents, and does not produce high sludge volumes that would require further treatment (Khamkure *et al.* 2021).

Research is currently focused on using novel adsorbents derived from different types of biomass, including different types of biopolymers, such as alginate (Chowdhury *et al.* 2019). Alginate is a biopolymer extracted from the outer cell wall of brown algae. It is usually prepared as calcium alginate. It is a polymer composed of unbranched chains of β-D-mannuronic and α-L-guluronic acids linked by $1\alpha \rightarrow 4$ bonds (Swain *et al.* 2013; Xiang *et al.* 2014). Alginate has been widely proven to be an

effective and efficient adsorbent for removing arsenic from contaminated water (Hassan *et al.* 2014; Ociński *et al.* 2016; Thomas-Busan *et al.* 2020). However, its properties as an adsorbent can be improved if its external surface is modified with chemical agents that can enhance its selectivity for some target pollutants, such as arsenic present in drinking water. Furthermore, if alginate is used as a small particle size adsorbent, it can significantly improve the removal of this contaminant.

On the other hand, arsenic is strongly adsorbed on mineral surfaces containing trivalent metals (such as Al and Fe) in the natural environment. Based on this evidence, alternative technologies have been developed in recent years to verify the high affinity of Fe(III) for arsenic ions in various adsorbents (Swain *et al.* 2013; Lalhmunsiama *et al.* 2017; Zang *et al.* 2021). However, it has also been reported that nanoscale Fe intensifies its functional and surface properties, providing bonds with functional groups that favor adsorption (Habuda-Stanić & Nujić 2015; Sousa *et al.* 2015). In addition, the use of polymeric adsorbents with proven efficacy in the removal of As(V), such as calcium alginate (Chowdhury *et al.* 2019), provides advantages for its use as a support for iron nanoparticles (FeNPs), which also provides the advantage of nanoparticle recovery, and as an adsorbent for these ions. In this context, the encapsulation of FeNPs in calcium alginate microspheres will provide a higher removal efficiency of As(V) from aqueous solutions because of this composite material's structural and surface properties. Based on the above, the main contributions of this work lie in the use of a simple method for obtaining iron nanoparticles (FeNPs) and their homogeneous encapsulation in alginate at low FeNPs concentrations. This will make it possible to produce more effective and competitive adsorbents than those used conventionally, reducing their cost and maintaining their efficiency for removing As(V) ions. In addition, to the best of our knowledge, there are no reports regarding the use of alginate microspheres prepared by these methods for removing As(V), and our hypothesis is that by using this particle size, together with the modification of its surface with FeNPs, the adsorption kinetics will be significantly improved. Furthermore, alginate microspheres can be used without major hydraulic and technical problems in continuous water treatment operations for human consumption.

Therefore, the main objective of this work was to evaluate the arsenate removal using calcium alginate microspheres with encapsulated iron nanoparticles and to compare its efficiency with that of the material without FeNPs, by determining the kinetic, equilibrium, and thermodynamic parameters of each adsorbate-adsorbent system.

MATERIALS AND METHODS

Materials and reagents

The alginate microspheres were obtained from sodium alginate (Sigma-Aldrich), and the stock solution was formulated from sodium arsenate heptahydrate ($Na_2HAsO_4.7H_2O$ Sigma) dissolved in deionized water. The calcium solutions used to synthesize the microspheres were prepared from $CaCl_2.2H_2O$ (Merck) dissolved in deionized water. The FeO suspensions used for gel encapsulation were prepared from $FeSO_4.7H_2O$ (Merck) dissolved in deionized water, using a NaOH solution for pH adjustment. All the reagents were used without further purification.

Calcium alginate microspheres preparation

The alginate microspheres were prepared using sodium alginate as a precursor, utilizing a 2% (w/v) sodium alginate solution in deionized water. Subsequently, the solution was placed on a stir plate for 3 h at 50 °C until a transparent and viscous solution was observed and allowed to stand for 24 h. Additionally, 500 mL of 150 mM calcium chloride solution was prepared. Next, the microspheres were prepared using a drip system on a $CaCl_2$ solution, and the mixture was shaken at 60 rpm to allow the formation of microspheres. Once formed, the microspheres were agitated for 24 h. Subsequently, the microspheres were separated from the solution and washed several times with deionized water to produce deprotonated calcium alginate microspheres (AlgN). Finally, the alginate spheres were dried in an oven at 35 °C.

Iron nanoparticles encapsulation in calcium alginate microspheres

A solution of 1 g $FeSO_4.7H_2O$ in 100 mL of deionized water was prepared, adjusting the pH from 10 to 12 with NaOH and adjusting the volume to 200 mL with deionized water. The solution was then introduced into a conventional microwave oven (600 W, 2,450 MHz) for 10 min; then, the produced iron nanoparticles (FeNPs) were washed several times with deionized water. For the encapsulation of iron nanoparticles in alginate microspheres, 1 g of sodium alginate was mixed with 2 mL of the Fe nanoparticle suspension prepared previously until a homogeneous distribution of iron nanoparticles in the suspension was achieved. The solution was then left to rest for 24 h. Next, microspheres were prepared as described above to obtain

Ca-alginate microspheres with encapsulated Fe nanoparticles (AlgFe). Finally, both AlgN and AlgFe microspheres were dried, sieved, and stored in a desiccator for further use in adsorption experiments.

Adsorbent characterization

The surface morphologies of the AlgN and AlgFe materials were examined using high-vacuum scanning electron microscopy (SEM) by a JEOL JSM IT300 scanning electron microscope operated at 20 kV, with a BRUKER XFlash6130 energy dispersive X-ray spectrometer (EDS) attached. Besides, the elements present in the structure of the microspheres, before and after As(V) adsorption, were determined using elemental microanalysis by EDS. Similarly, the size and form of iron nanoparticles were determined using this method. In addition, both adsorbents were analyzed, before and after arsenate adsorption, by Fourier Transform Infrared Spectroscopy (FTIR) (Bruker® Model Tensor 27 Spectrophotometer), in the range of 400 and 4,000 cm^{-1}, to determine functional groups on the surface of the adsorbents. Furthermore, the Zeta Potential (δ) was measured by a Nanobrook 90plus Zeta-meter to determine the surface charge and the Point of Zero Charge (pH_{PZC}) of the adsorbents.

Influence of contact time on As(V) adsorption

To determine the influence of the contact time on the adsorption of As(V) batch experiments were carried out using both adsorbents: AlgN and AlgFe. These experiments were performed in centrifuge tubes by contacting 100 mg of each adsorbent, separately, with 10 mL of a 10 mg/L $Na_2AsO_4.7H_2O$ solution. The tubes were shaken at 100 rpm in a reciprocal shaker at 25 °C for different contact times, ranging from 5 to 480 min. After the contact time was reached, the solution was filtered, and the supernatant was placed in vials for arsenic analysis by atomic absorption spectroscopy (AAS) using a hydride generation system. The amount of As(V) adsorbed on the alginate microspheres was calculated from the initial concentration of the solution (C_0) and the equilibrium concentration in the solution (C_e), according to equation S1 (Eq. S1).

Adsorption experiments were performed three times to determine the results' reproducibility, and the mean values were reported. Control experiments showed that arsenic did not adsorb on the walls of the centrifuge tubes, and analyte loss was not detected.

Effect of adsorbent dose

In order to determine the effect of the adsorbent dose on As(V) removal, contact experiments with AlgN and AlgFe and arsenate aqueous solutions were carried out. First, adsorbents samples were separately placed in centrifuge tubes ranging from 0.1 to 1 g, and 10 mL of a 10-mg/L $Na_2AsO_4.7H_2O$ solution were added. Next, the tubes were shaken as mentioned above until the system's equilibrium was reached, and the supernatant was analyzed by AAS.

Influence of pH on As(V) removal

To establish the pH value at which the alginate microspheres have a more significant As(V) removal and to determine the influence of this parameter on the adsorbent material, adsorption experiments were carried out using AlgN and AlgFe as adsorbents. Different As(V) solutions with pH values between 3 and 9 were prepared. The pH values of solutions were adjusted using 0.1 M HCl or 0.1 M NaOH solutions. These tests were carried out using the adsorbent dose obtained in the previous experiment; this amount of adsorbent was placed in centrifuge tubes with 10 ml of As(V) solutions at different pH values and stirred under the same conditions mentioned above. At the end of the contact equilibrium time, the solution was filtered, and the supernatants were placed in vials and analyzed using AAS.

Adsorption isotherms

Batch-type adsorption experiments were performed to determine the arsenate adsorption isotherms, using AlgN and AlgFe as adsorbents and As(V) aqueous solutions at different concentrations, ranging from 10 to 500 μg/L. Besides, different temperatures (25, 35, and 45 °C) were tested to determine the effect of this parameter on both adsorbate-adsorbent systems. For this purpose, doses of each adsorbent were separately contacted with 10 mL of $Na_2AsO_4.7H_2O$ solutions at the different concentrations mentioned above. The pH of the arsenate solution was 6 for both adsorbate-adsorbent systems. The tubes were shaken as mentioned above until the system's equilibrium was reached, and AAS was used to analyze supernatants.. Finally, the adsorbate concentrations in the solid were calculated according to Eq. S1.

RESULTS AND DISCUSSION

Adsorbent characterization

The SEM study allowed us to determine the morphological aspects of the microscopic areas of the adsorbents and their semi-quantitative elemental microanalysis. Figures 1–3 show the micrographs of AlgN and AlgFe, where surface morphological differences caused by FeNPs encapsulation can be noted. In the case of AlgN (Figure 1(a) and 1(b)), microspheres of a size ranging from 400 to 500 μm with a smooth, concave laminar surface were observed. Because adsorption is a surface phenomenon, a small particle size offers a larger and more accessible surface and, generally, a higher adsorption capacity; thus, this material could have good arsenate adsorption behavior. In addition, an elemental microanalysis (EDS) of AlgN showed the presence in different concentrations of C, O, Cl, Ca, and Na in the structure of the alginate microspheres.

Conversely, the AlgFe sample (Figure 1(c)) reveals microspheres with a rough and porous surface; this morphology can be attributed to the chemical treatment that was carried out. It is well known that when adding an iron salt to the water, it tends to acidify because of hydrolysis, so the surface morphology of the AlgN microspheres suffered changes during the modification process with FeNPs, becoming more irregular. Similar behavior has been reported for Ca-alginate beads modified with Thiosalicylic acid (Alp Arıcı *et al.* 2020). The development of a porous textured surface makes the surface more susceptible to activating its functional groups, and the surface area is also increased, favoring intraparticle diffusion and As(V) removal on encapsulated FeNPs (Lim *et al.* 2009). Moreover, since adsorption is a surface phenomenon, reducing the adsorbent's particle size causes a comparatively more extensive and accessible surface area (development of more pores) and, therefore, a higher adsorption capacity. The spheres showed a relatively homogeneous grain size distribution, ranging from 400 to 500 μm. In addition, SEM micrographs were taken to FeNPs to corroborate their nanometric size; results showed nanoparticle sizes ranging from 60 to 90 nm (Figure 2(a)).

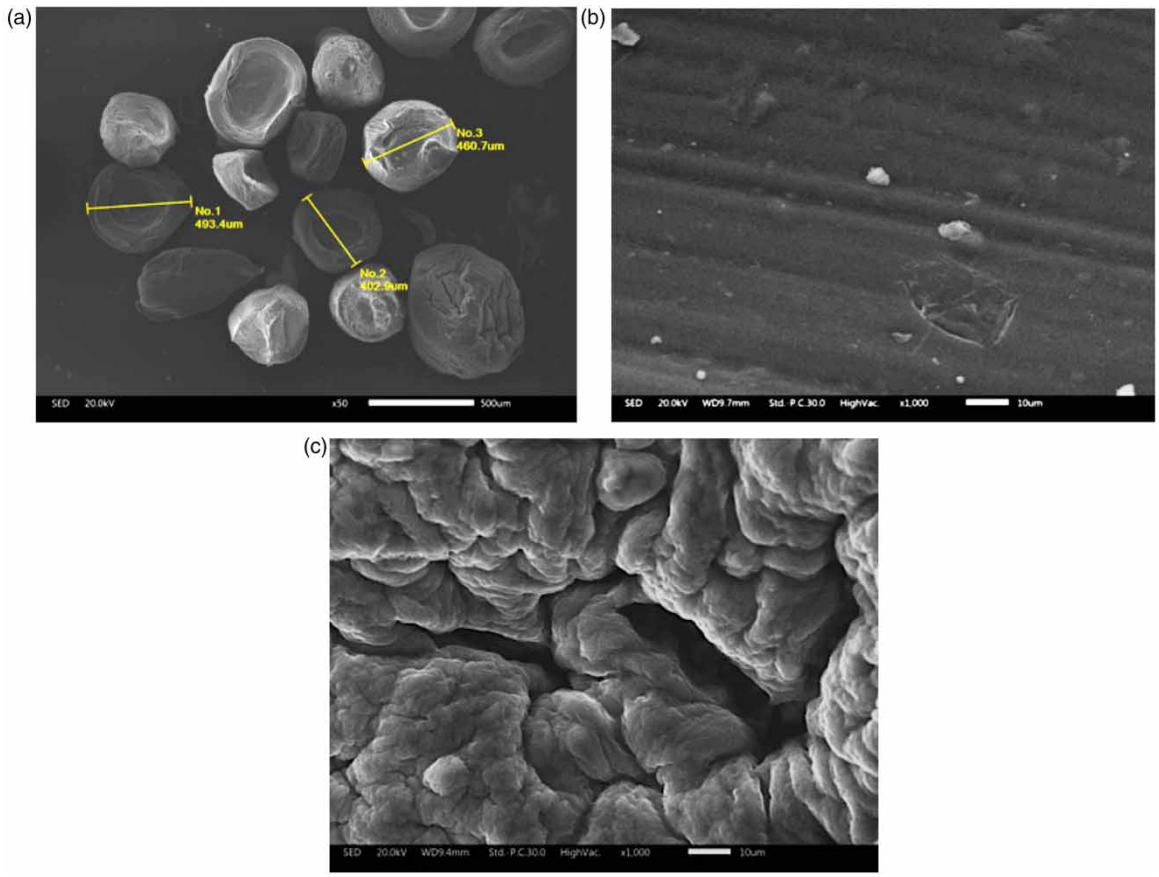

Figure 1 | SEM micrographs of AlgN and AlgFe samples: (a) AlgN microspheres observed at 50x; (b) AlgFe microspheres observed at 1000x; (c) AlgFe microspheres observed at 1000x.

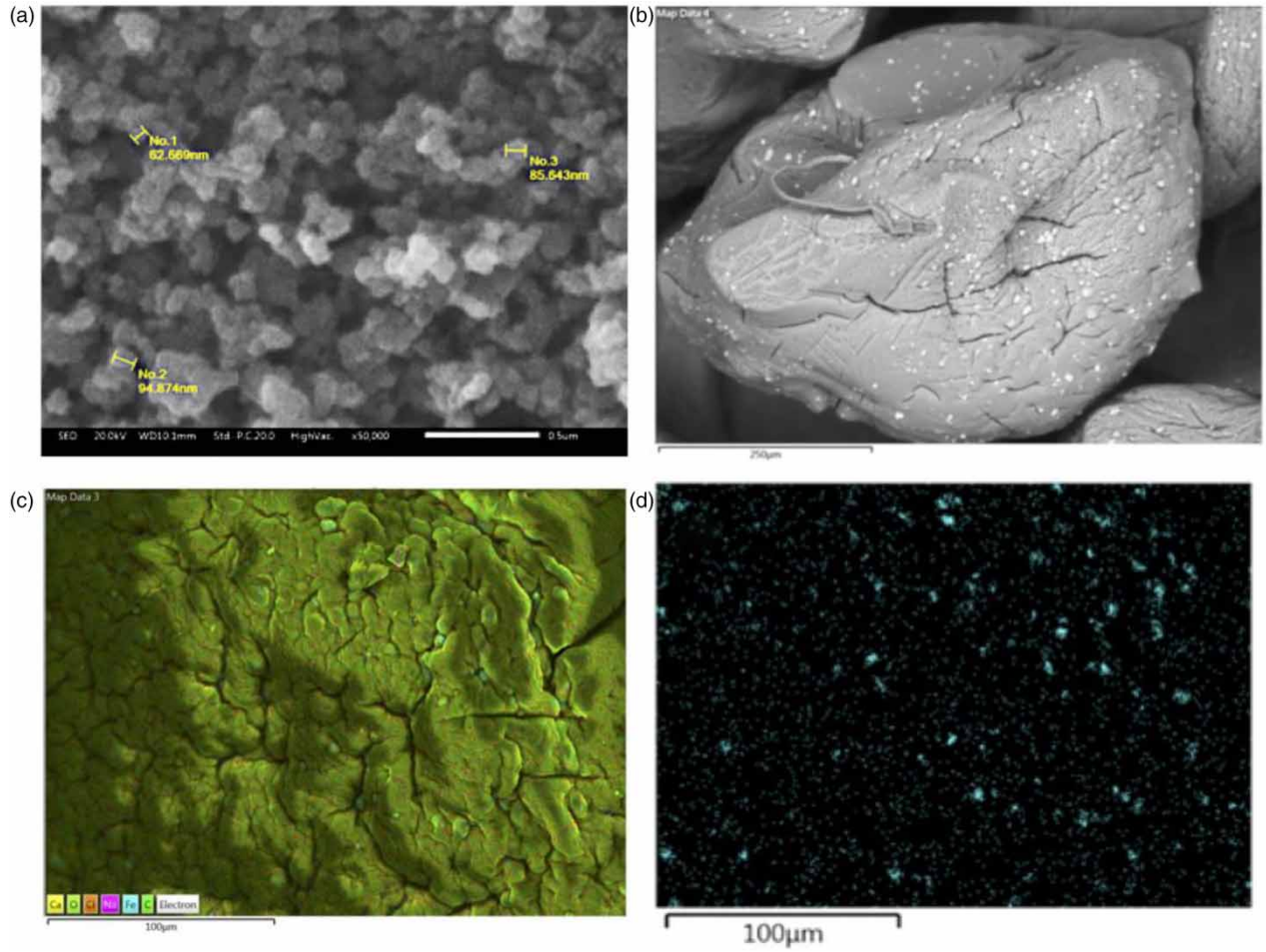

Figure 2 | SEM micrographs of (a) FeNPs in suspension; (b) AlgFe microspheres; (c) total elements mapping on AlgFe; (d) Fe-mapping on AlgFe.

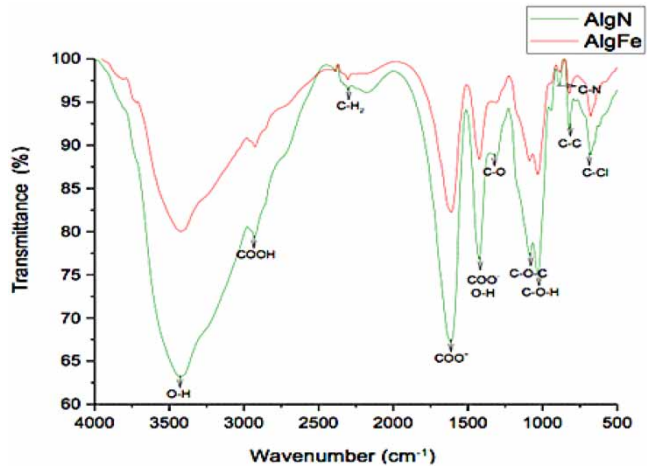

Figure 3 | FTIR spectrograms of AlgN and AlgFe.

Figure 2(b)–2(d) show the microspheres' micrographs after FeNPs encapsulation (AlgFe). It can be observed that the external surface of AlgFe has a small number of Fe nanoparticles (white dots), as shown in SEM images (Figure 2(b)) since most of them were encapsulated. In order to know the adsorbent composition, a semi-quantitative elemental analysis (EDS) was

performed, showing the following composition for AlgFe (as weight percentage): 44% of O and 43.2% of C, followed by 8.3% Ca, 3.1% of Cl, and 0.1% of Na. Figure 2(c) shows a general mapping and relative distribution of AlgFe main components. In this case, iron was present at 1.4%. This fact indicates that the AlgN modification process incorporates Fe nanoparticles in the adsorbent's internal and external structure. Bright blue dots shown in Figure 2(d) indicate that significant amounts of FeNP's are located within the internal structure of the microspheres, corroborating the FeNPs encapsulation by Ca-alginate. Similar observations have been reported to encapsulate heme iron into alginate beads (Valenzuela *et al.* 2014). Also, some FeNPs were found on the outer surface of AlgFe, where a relatively homogeneous distribution was observed (Figure 2(d)). The FeNPs distribution on alginate microspheres could represent an advantage for application in adsorption processes since the outer FeNps present on the external surface of the adsorbent could enhance adsorption capacity and diversify its removal mechanisms.

Elemental mapping and microanalysis were performed on AlgN and AlgFe samples after arsenate adsorption (Figure S1). Figure S1a shows the complete elemental mapping of AlgN after As(V) removal. Figure S1b shows arsenic mapping (in the same sample field as Figure S1a), where the presence of arsenic (blue dots) retained on the AlgN surface, in a relatively homogeneous form, was detected. According to the EDS analysis, an approximate content of 0.2% (w/w) was determined. This behavior suggests that most of the functional groups located on the adsorbent's external surface are involved in the adsorption of arsenate. The EDS analysis of the AlgF sample after arsenate adsorption is shown in Figure S1c, where the total elements present in the adsorbent can be noted. Moreover, Figure S1d shows the arsenic mapping for the same sample field shown in Figure 3(c). It was found that the As is significantly retained on the AlgFe external surface. However, the brighter purple dots observed in this micrograph (Figure S1d) suggest a strong interaction between encapsulated FeNPs and arsenate ions. In addition, approximate arsenic content of 0.75% (w/w) in AlgFe was determined; this suggests higher arsenate adsorption capacity of AlgFe than AlgN and indicates that FeNPs enhance As(V) removal.

Functional groups were determined by FTIR analysis of AlgN and AlgFe samples. The results are shown in Figure 3. Absorption bands characteristic of hydroxyl, methyl, ester, ether, and carboxyl groups were found. These groups are distinctive of alginate, present in carbohydrate compounds, reflecting their complex organic structure (Daemi & Barikani 2012; Xiang *et al.* 2014). In Figure 3, the bands at 3,423.72 cm^{-1} wavelengths correspond to the O-H stretching and the intermolecular hydrogen bond; bands at 2,848.42 and 2,856.26 cm^{-1} correspond to the CH stretching of the -CH_3 group present in the pyranoid ring; and the band at 2,926.89 cm^{-1} corresponds to COOH group (Daemi & Barikani 2012). Likewise, carboxyl groups are found at peaks close to 1,613.20 cm^{-1} (COO-), corresponding to symmetrical stretching vibration, and also near to 1,424.46 cm^{-1}, which are attributed to asymmetric tension vibration (COO-) (Swain *et al.* 2013; Xiang *et al.* 2014).

AlgN microspheres also show tension bands of CO at 1,308.67 cm^{-1} and bands corresponding to the C-O-C and C-O-H vibrations at 1,089.29 and 1,032.21 cm^{-1}, respectively, from a glycosidic bond (Flores-Garay *et al.* 2016). In addition, the band at 676.72 cm^{-1} indicates the existence of a carbon skeleton (C-C), and the band at 424.62 cm^{-1} reveals groups derived from chloroalkanes (C-Cl) (Ghani *et al.* 2016). Thus, the results obtained in the FTIR analysis for AlgN are consistent with the characterization studies reported in the literature (Xiang *et al.* 2014; Flores-Garay *et al.* 2016), which demonstrates that alginate has a hydrophilic character due to its carbohydrate-derived compounds.

Figure 3 also shows the comparison between the FTIR spectrograms of AlgN and AlgFe. The similarity between both spectra is mainly due to the prevalence of coincident groups in the calcium alginate microspheres. However, different band intensities are observed; these differences can be attributed to FeNPs modification of AlgN; these changes on band intensities indicate the interaction of functional groups, such as (COOH), (O-H), (COO-), (C-O-C), and (C-O-H), with iron. This behavior can be attributed to ion exchange processes during the FeNPs encapsulation (Lv *et al.* 2013). Based on the above, it can be suggested that different adsorption mechanisms may exist because a small number of iron nanoparticles are present on the external surface of AlgN. The alcohols (O-H), ester (C-O-C), ether (C-O-H), and carboxylic acid groups (COOH) show the most significant variation in absorption bands, indicating that they are involved in the FeNPs binding process (Swain *et al.* 2013; Flores-Garay *et al.* 2016). Such changes in band intensities can be attributed to the ion-to-ion displacement, which generates practically the same spectrum form (Flores-Garay *et al.* 2016). The wavelengths ranges of the bands where the greatest changes were found are: 3,423.72–3,031.96 cm^{-1}; 2,926.89–2,923.14 cm^{-1}; 1,613.20–1,610.65 cm^{-1}; 1,424.46–1,422.01 cm^{-1}; 1,089.29–1,087.52 cm^{-1} and 1,032.21–1,031.07 cm^{-1}. Additionally, hydrogen bonds can be seen in the bands at 3,423.72 and 3,031.96 cm^{-1}, which involve water molecules and generate O-H stretching vibrations; these bands are related to Fe-OH bonds in the AlgFe spectrum (Figure 3) (Ayoob *et al.* 2008; Flores-Garay *et al.* 2016). The bands between 2,926.89 and 2,923.14 cm^{-1} in the AlgFe spectrum are related to the COO-Fe carboxylic acid bonds. Similarly,

the bands between 1,613.20–1,610.65 cm^{-1} and 1,424.46–1,422.01 cm^{-1} can be attributed to symmetric and asymmetric stretches of carboxyl ions (COO-) (Nazari & Halladj 2014). Moreover, for AlgFe, the band range between 1,424.46 and 1,422.01 cm^{-1} denote the characteristic stretch modes of Fe = O bonds. It was also possible to observe the formation of a small band in AlgFe around 580 cm^{-1}, related to Fe-O bonds in magnetite (Lim *et al.* 2009). This evidence of iron bonds, together with the magnetic properties of the alginate microspheres with FeNPs, suggests that the iron present in this composite is magnetite. Also, the mechanism of Fe adsorption on alginate is chemical and is, therefore, mostly irreversible (Ayoob *et al.* 2008).

FTIR analysis was performed on AlgN and AlgFe after arsenate removal. The results are presented in Figures 4 and 5 for AlgN and AlgFe, respectively. A decrease in band intensities for specific functional groups was observed; such reduction after contact is associated with the system's arsenate adsorption capacity. The bands associated with this decrease in intensities correspond to the hydroxyl and carboxyl functional groups; therefore, it can be established that such functional groups are involved in removing As(V) for both adsorbents. This adsorption behavior is also observed by the decrease in the intensity of the band at 3,422.64 cm^{-1}, formed by the O-H bonds; this is easily explained since O-H and arsenate ions have very similar dimensions, and they can exchange (Nazari & Halladj 2014). Moreover, arsenate ions and hydroxyl groups can also interact electrostatically to form hydrogen bonds. A decrease in the bands at 2,923.14, 1,610.65, and 1,422.01 cm^{-1} wavelengths, corresponding to COOH groups, was also observed for AlgN and AlgFe (Figures 4 and 5), indicating a strong interaction between these groups and arsenate ion on both adsorbents. Similarly, a reduction in the 1,087.52 cm^{-1} band intensity, corresponding to C-O-C ether groups, and even in the band at 676.93 cm^{-1} assigned to C-C was also found, and the C-As link can also be observed (Xi & Chen 2014).

An absorption band assigned to a functional group increases proportionally with the number of times the functional group exists within the molecule. Therefore, by decreasing the bands' intensity, it can be established that the functional group has reduced its presence in the analyzed sample or is forming some bond or interaction with other groups present in it. The results obtained from the FTIR analysis agree with those reported previously (Benyoucef & Amrani 2011), where it was established the O-H and COOH groups as the main ones responsible for the adsorption. Besides, the small band related to the Fe-O bond in AlgFe (Figure 5) has completely disappeared in the arsenate-loaded adsorbent (AlgFeAs), indicating interaction with such bonds and the anionic adsorbate. Also, the bands related to Fe=O groups decreased their intensities. This behavior indicates that FeNPs in the AlgFe microspheres play an essential role in As(V) removal.

On the other hand, the Zeta Potential (ζ) measures the shear plane's electrical potential in suspended particles. The variation in ζ as a function of pH for AlgN and AlgFe is shown in Figures S2a and S2b, respectively. The Point of Zero Charge point (pH_{PZC}) of both adsorbents can be established by evaluating the variation in zeta potential. The pH_{PZC} value for the AlgN system was 2.2 (Figure S2a), mainly attributed to the presence of ionized carboxyl groups. For the AlgFe adsorbent, the pH_{PZC} was 5.35 (Figure S2b). A positive surface charge in the AlgFe sample can occur at pH values lower than 5.35, which favors the adsorption of anions on its surface by Coulomb attraction. Conversely, when the pH values are higher

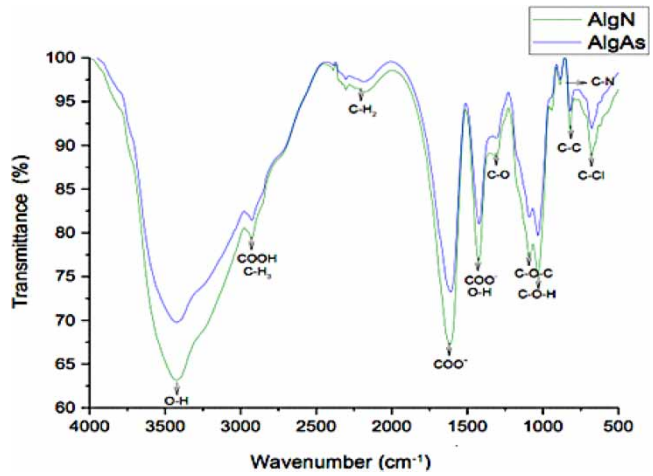

Figure 4 | FTIR spectrograms of AlgN microspheres before and after arsenate adsorption (Alg-As).

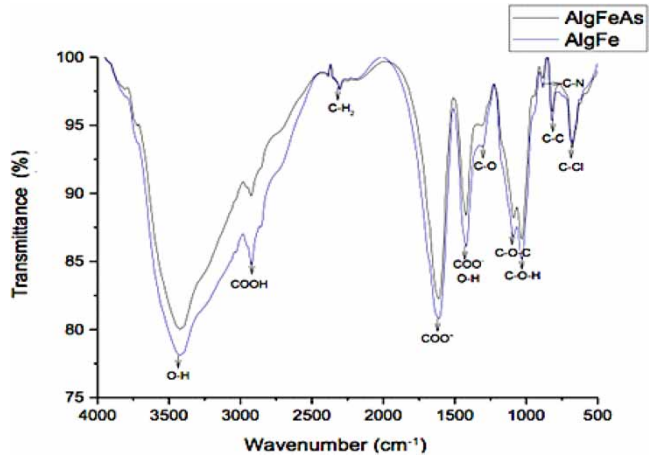

Figure 5 | FTIR spectrograms of AlgFe microspheres before and after arsenate adsorption (AlgFeAs).

than 5.35, the surface charge is negative, making anion removal hard to occur by this mechanism (Dayananda *et al.* 2014). When the AlgN microspheres were modified using an iron salt ($FeSO_4$), some of the negative charges on the surface of the material were neutralized, producing a more suitable surface for the removal of the arsenic anions. Different behavior of ζ can be observed in the case of AlgFe (Figure S2b), which can be associated with a more significant presence of H^+ ions since the modification with the iron causes neutralization of charges in the unmodified material. Consequently, the obstacle to the diffusion of negatively charged arsenate ions reduces, resulting in a more active surface (Gong *et al.* 2005; Wang *et al.* 2014a). Moreover, the tendency to form complexes between arsenates and iron increases, which suggests that arsenate ions coordinate with Fe(III) ions; therefore, the formation of hydrolyzed As(V) species is favored since both their solubility and the competitive effect decrease significantly. Accordingly, the functional groups come into contact easily with the hydrolyzed species in their anionic form (Dutta *et al.* 2012; Safarik & Safarikova 2013).

As(V) adsorption kinetics

The adsorption kinetics results for both systems at different contact times are shown in Figure 6. In both cases (AlgN and AlgFe), it can be observed how the removal of As(V) as a function of time can be divided into two parts, comprising rapid adsorption in the first minutes of contact and, later, slow adsorption until reaching the adsorption equilibrium. The equilibrium time for the AlgN was 120 min, removing 49.4% of initial arsenate ions. For the AlgFe microspheres, a removal of 65.3% of As(V) at an equilibrium time of 120 min was observed. In most cases where the electrostatic forces between the adsorbate and the adsorbent act as an adsorption mechanism, it can be considered that in the first stage of removal

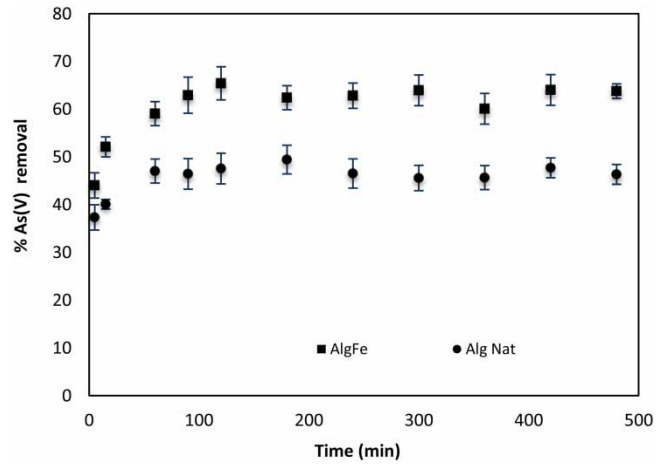

Figure 6 | Removal of As(V) by AlgN and AlgFe as a function of time (min).

(which is significantly fast), these forces have a strong influence on the process. Therefore, significant differences are observed in the adsorption kinetics for both adsorbents in this initial stage, particularly for AlgN, since slightly faster adsorption can be observed at this point (Figure 6). Similarly, for the second stage (which is usually slow) the decrease in the ionic strength and the adsorbate concentration gradient causes the speed of the process to decrease. As observed, the slight differences in the first adsorption stage can be attributed to more significant interaction between the As(V) ions and the functional groups present on the external surface of the AlgN. At the same time, the higher removal efficiency observed when using AlgFe can be attributed to a more active interaction between arsenate ions and FeNPs in all stages of the process.

The data obtained in these experiments were fitted to the well-known Elovich, Lagergren's Pseudo-first-order, and Pseudo-second-order empirical models by non-linear regression analysis (Lagergren 1898; Ho *et al.* 2000; Low 1960). Table 1 specifies As(V) sorption kinetic parameters for AlgN and AlgFe. Primarily, As(V) sorption kinetic data were better described by the Pseudo-second-order model, with $R = 0.9943$, and $R = 0.9952$ for AlgN and AlgFe, respectively. This fact suggests that both adsorbents remove arsenic through a chemisorption mechanism, implicating valence forces resulting from ion exchange or sharing pairs of electrons between the solute and the microspheres' functional groups (covalent bond) (Ho & McKay 2002). Furthermore, a higher adsorption rate (K_2) was obtained for AlgN microspheres, implying that As(V) sorption in this adsorbent was faster than for AlgFe, considering the whole range of adsorption kinetics process. This fact reveals a better interaction of arsenate ions in the AlgN system in terms of diffusion, and it also suggests that intraparticle diffusion may be a limiting step in the removal kinetics of As(V) when AlgFe is used. The removal of arsenates has been reported using hydrous iron oxides immobilized in calcium alginate beads (HIO-P-Alg) (Sigdel *et al.* 2018), finding that such modification improves the adsorption rate of the alginate beads. In this work, the global adsorption rate decreases slightly for AlgFe, and the above suggests that the method of immobilization of iron on alginate plays an essential role in adsorption kinetics. Furthermore, it is important to emphasize that the adsorption equilibrium time is significantly shorter compared to HIO-P-Alg. Moreover, similar results to those described here have been reported previously for the removal of As(V) ions using Ca–alginate-entrapped nanoscale zero-valent iron (NZVI) (Bezbaruah *et al.* 2014). However, lower rate constants (at similar experimental conditions) were found for NZVI. Therefore, the differences in adsorption rate constants when comparing NZVI and AlgFe could be mainly attributed to the particle size of the AlgFe microspheres. Finally, it can be established that the arsenate adsorption kinetics is significantly fast, and encapsulation of FeNPs by Ca-alginate microspheres enhanced kinetic performance compared to other iron oxide immobilization methods.

Effect of adsorbent dose

The effect of the adsorbent dose on arsenate removal can be seen in Figure S3 for AlgN and AlgFe. It can be noticed that maximum removal is achieved at an adsorbent concentration of 20 g/L of AlgN. For the AlgFe adsorbent, removal of up to 90% at a 70-g/L dose was achieved. Increasing the adsorbent dose in the AlgN system does not significantly increase its ability to remove arsenate. However, in the AlgFe system, an increase in arsenate removal was observed as adsorbent dose also increases; this behavior can be associated with the FeNPs encapsulation in AlgFe, which corroborates that the FeNPs have direct interaction with Arsenate ions. The above also indicates that, by increasing the concentration of FeNPs in the adsorption system, As(V) ions removal is significantly improved. On the other hand, even though the adsorbent dose for AlgFe progressively increases, it was observed that As(V) removal does not increase beyond a 70 g/L dose, which can be attributed to the microspheres agglomeration or an increase in solution viscosity (Lavanya *et al.* 2021), restraining the ions' diffusion towards the adsorption sites.

Influence of pH on As(V) removal

The solution's pH is an essential parameter to assess in adsorption processes because it significantly influences the solution's composition, ionization degree, chemical speciation, and adsorbent properties. For example, it is known that at low pH

Table 1 | Kinetic parameters of As(V) adsorption by AlgN and AlgFe microspheres

	Pseudo-first-order			Pseudo-second-order			Elovich		
Adsorbent	K_L (min^{-1})	q_e (mg/g)	R	K_2 (g/mg·min)	q_e (mg/g)	R	α (mg/g·min)	β (g/mg)	R
AlgN	0.3108	0.0337	0.9877	19.42	0.0343	0.9943	0.000028	1.0128	0.8556
AlgFe	0.2250	0.0450	0.9858	9.03	0.0460	0.9952	0.000044	1.0163	0.8301

values, H_3AsO_4 and $H_2AsO_4^-$ are the predominant As(V) species in aqueous solution (Santos *et al.* 2016). This parameter also has a significant influence on the surface chemistry of the adsorbent. Figure 7 shows the pH's influence on arsenate removal with AlgN and AlgFe microspheres, in a pH range from 3 to 9. Removal of up to 68.86 and 90% was observed for AlgN and AlgFe, respectively, at slightly acidic conditions. For the case of AlgFe, this behavior is attributed to the concentration of H^+ ions since the negative charges on the adsorbent surface were neutralized. This fact, in turn, reduces the obstacle to the film diffusion of negatively charged arsenic ions and results in a more active surface for adsorption (Gong *et al.* 2005; Wang *et al.* 2014a). As the solution's pH raised (pH $\geq$ 7), the functional groups become negatively charged, producing the repulsion of the predominant anionic species of As(V) in the aqueous medium (H_3AsO_4 and H_2AsO_4). These changes in solution and surface chemistry inevitably resulted in low removal efficiency. Competition for active sites in the adsorbent, along with electrostatic repulsion, could be responsible for the observed behavior, as previously reported (Dutta *et al.* 2012; Safarik & Safarikova 2013). Moreover, in the AlgFe system, competition between As(V) and OH- ions and arsenate solubility decreases at low pH values. This behavior promotes arsenate hydrolyzed species formation and facilitates contact between the adsorbent's functional groups and the solute, favoring the arsenate ions to coordinate with the Fe(III) ions present in the material. The FeNPs at this pH range are mainly present as Fe_2O_3 (Safarik & Safarikova 2013).

Furthermore, α-L-guluronic and β-D-manuronic acids, naturally present in alginate, contain carboxylic acids in their structure, and their pKa values were reported between 3.4 and 3.9 (Xiang *et al.* 2014); this fact implies that the adsorbent has a positive charge at pH values lower than these values, which results in higher adsorption of the anion. Therefore, based on these results and considering the typical pH values of As(V) polluted waters, a pH value of 6 was chosen for further experiments.

According to the pH effect on As(V) adsorption and the FTIR analyses, the primary adsorption mechanism is given by the exchange between hydroxyl ions and the arsenate ions for both AlgN and AlgFe systems. A slight increase in the supernatant's pH after the adsorption process allowed verification of this mechanism. The following reactions can represent these mechanisms (Guo *et al.* 2015):

$$COOH + H_2AsO_4^- \Rightarrow HAsO_4 + 2OH^- \quad (1)$$

$$\delta - Fe(OH)_2 + H_2AsO_4^- \Leftrightarrow \delta - Fe_2HAsO_4 + 2OH^- \quad (2)$$

However, for the AlgFe system, another mechanism given by the chemical reaction of iron and the acid form of As(V) could also be observed since this species forms stable coordination compounds with iron oxides, which can be represented as follows (Hernández Ordáz *et al.* 2013):

$$\delta - FeOH + H_2AsO_4^- \Leftrightarrow \delta - FeH_2AsO_4 + H_2O \quad (3)$$

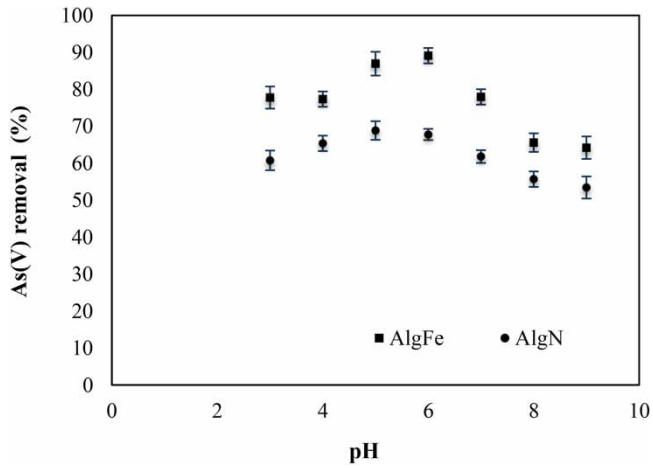

Figure 7 | pH effect on As(V) adsorption onto AlgN (•) and AlgFe (■).

The products are ferric arsenate and water, as this iron compound is often considered the most stable because it has a low solubility product (Hernández Ordáz *et al.* 2013). These results are satisfactory for the method's applicability since no significant iron concentrations were found in the supernatants of the adsorption process; thus, it can be considered a primary sorption mechanism for encapsulated FeNPs. This fact indicates the low leaching of the metal adhered to the adsorbent, which is favorable for its application in an aqueous medium. It is also important to mention that the iron-modified alginate microspheres (AlgFe) showed magnetic properties, providing them with an advantage in their recovery when treating arsenic-polluted waters.

As(V) adsorption isotherms

In Figures 8 and 9, the influence of temperature on the arsenate adsorption isotherms can be observed for AlgN and AlgFe, respectively. The purpose of evaluating the adsorption of As(V) ions using AlgN and AlgFe at different temperatures was to determine the effect of this parameter on the adsorption capacity; since it has been observed that groundwaters with high levels of arsenic generally present high temperatures. Therefore, these adsorbents could be applied directly in water supply treatment operations at such temperatures. A slight increase in the adsorption capacities can be noticed as the adsorbate-adsorbent systems' temperature also increases. Heat produces a rise in kinetic energy of the As(V) ions movement through the outer boundary layers and adsorbents' internal pores, so the increase in adsorption capacities may be associated with this phenomenon. Based on the above, it can also be suggested that an endothermic process could be controlling As(V) sorption by AlgN and AlgFe (Wei *et al.* 2011; Geethamani *et al.* 2013).

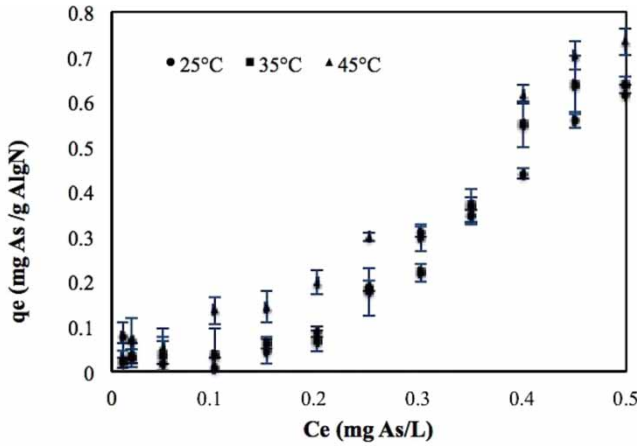

Figure 8 | As(V) adsorption isotherm for AlgN at 25 °C, 35 °C and 45 °C.

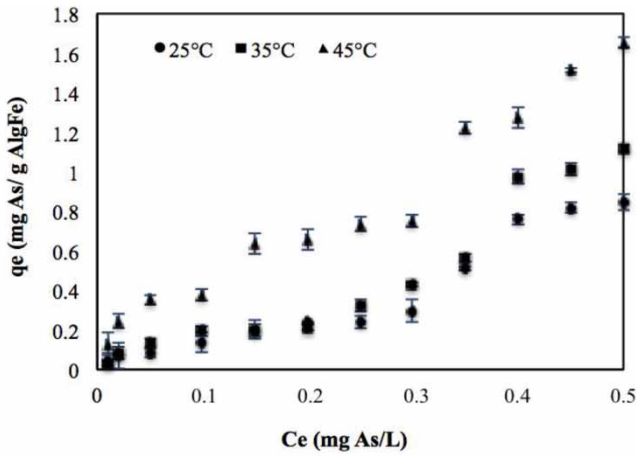

Figure 9 | As(V) adsorption isotherm for AlgFe at 25 °C, 35 °C and 45 °C.

Both adsorbate-adsorbent systems (AlgN and AlgFe) have an S-shaped isotherm, characteristic of mesoporous adsorbents, and involve cooperative adsorption with various activation energies. In this case, the initial behavior consists of forming a monolayer, followed by multilayer formation until reaching a certain thickness. This behavior supports the presence of a rough adsorbent in which the initial monolayer leaves many gaps, which end up saturating with adsorbate until reaching capillary condensation or the appearance of the hysteresis cycle (the filling process of the mesopores). The origin of the hysteresis is due to various factors, such as the pore geometry, or can also cause the adsorption-desorption cycle to be reversible or not (Hernández Ordáz *et al.* 2013; Guo *et al.* 2015). However, for the case of AlgFe at 45 °C (Figure 9), the shape of the isothermal curve changes significantly, taking the form of an H-type isotherm, indicating a high-affinity system due to the strong attractions between the adsorbate and the adsorbent (Giles *et al.* 1974a, 1974b). This behavior is indicative of the effective interaction between FeNPs encapsulated in Ca-alginate and arsenate ions since a higher temperature favors intraparticle diffusion, which also facilitates contact between the As(V) ions and FeNPs.

As(V) adsorption isotherms data were fitted to the well-known Freundlich, Langmuir and Langmuir-Freundlich isotherm models using a non-linear regression analysis. Tables 2 and 3 lists As(V) equilibrium parameters, obtained from isotherms data, for AlgN and AlgFe, respectively. The Freundlich model better fitted AlgN isotherm data (Table 2). This model is well-known for describing sorption systems with heterogeneous energies (Ye *et al.* 2012). Therefore, it can be established that significant adsorption at sites with different adsorption energy occurs when removing As(V) using AlgN, implying the presence of different As(V) adsorption mechanisms in this adsorbate-adsorbent system. Besides, the Freundlich parameter n_F indicates a favorable adsorption process for both systems. When n_F (adsorption intensity) values are higher than 1, favorable adsorption occurs in such a system, especially at high solute levels, but not for low solute concentrations. The values of this parameter for AlgN and AlgFe are higher than 1 in all cases, indicating a favorable sorption intensity at high concentrations and high temperatures.

Freundlich and Langmuir-Freundlich models can be used to describe well the AlgFe isotherm data; correlation coefficients (R) are listed in Table 3, and they ranged from 0.926 to 0.974. The Langmuir model showed lower R-values in all adsorbate-adsorbent systems. The Langmuir-Freundlich model is well known for describing adsorption equilibrium on heterogeneous surfaces; therefore, it can also be established that arsenate adsorption in AlgFe at different temperatures is heterogeneous. Arsenate adsorption, by similar adsorbents, has shown similar behavior as described above (Papageorgiou *et al.* 2008; Ramos-Vargas *et al.* 2018).

Furthermore, the maximum adsorption capacities (Q) calculated with the Langmuir model for AlgN ($R = 0.910$) and for AlgFe ($R = 0.8873$) were 0.989 mg/g and 1.217 mg/g, respectively, at 25 °C. A significant improvement in Q values can be observed for AlgFe, an evident effect of FeNPs encapsulation. At high temperatures (45 °C), this improvement in the

Table 2 | As(V) isotherms parameters using AlgN as adsorbent

	Langmuir			Freundlich			Langmuir-Freundlich			
T (°C)	Q	b	R	K_F	n_F	R	K_{LF}	a_{LF}	n_{LF}	R
25	0.9895	0.0017	0.9109	0.0010	0.99058	0.9688	0.00216	0.00004	0.8883	0.9500
35	1.0647	0.0016	0.8607	0.0018	1.08835	0.9142	0.01095	0.00003	0.6354	0.8177
45	1.1739	0.0019	0.9119	0.0014	1.00819	0.9650	0.00153	0.00005	0.98281	0.9623

Table 3 | As(V) isotherm parameters using AlgFe as adsorbent

	Langmuir			Freundlich			Langmuir-Freundlich			
T (°C)	*Q*	*b*	R	K_F	n_F	R	K_{LF}	a_{LF}	n_{LF}	R
25	1.2173	0.0022	0.8873	0.0049	1.2416	0.9296	0.0012	0.00001	1.0459	0.9576
35	1.6983	0.0019	0.8854	0.0053	1.2030	0.9268	0.0125	0.00001	0.6899	0.8957
45	3.7843	0.0012	0.9650	0.0167	1.3847	0.9713	0.0031	0.0001	1.0161	0.9743

adsorption capacity is more noticeable, which corroborates the more effective interaction of the arsenate ions with the FeNPs encapsulated in the microspheres and provides an advantage for applying this adsorbent, particularly in the treatment of arsenic polluted waters of geothermal origin.

Table 4 shows a comparison of the maximum adsorption capacities for As(V) ions (obtained from the Langmuir model) with similar adsorbents. When comparing various adsorbents, differences in experimental conditions were taken into account. As can be seen, the adsorption capacity of AlgFe is higher in some cases with similar experimental conditions; for example, it is higher than the adsorption capacity of alginate beads containing Fe and Mn oxides, which may be due to the immobilization method on these beads and to the Fe and Mn content. Similarly, the Q value for AlgFe is also higher than the magnetic xerogel monoliths, which can be attributed to the differences in the structure of the polymer used to immobilize the magnetic particles. It can also be observed that the Q value for AlgFe is competitive with some other adsorbents with higher porosity, as is the case with Iron-treated Biochar, where it is feasible that the difference in adsorption capacity is due to the biochar's higher surface area and the iron-modification of this adsorbent.

Even though the adsorption capacity of arsenate ions is lower for AlgFe compared to other adsorbents that have higher porosity and specific surface area, such as activated carbons (ACs), the advantage of AlgFe over ACs lies in the method of obtaining the adsorbent material since this implies less energy in its preparation process. In addition, the Q value is also higher in a very similar adsorbent such as magnetic nanoparticles impregnated chitosan beads. The difference, in this case, may be due to the FeNPs immobilization method; they were impregnated on the external surface of the alginate, which implies a better interaction between the FeNPs and the arsenate ions. Furthermore, the concentration of FENPs in the alginate may also be a factor that influences a higher Q value in this case. Therefore, although the AlgFe Q value is lower in some cases, this adsorbent has better adsorption kinetic parameters than most listed adsorbents (Table 4), which gives it a fundamental advantage in its subsequent application in adsorption columns; besides, the encapsulation of FeNPs ensures fewer iron losses due to leaching when removing As (V) from polluted waters. Under this context, the advantage of employing AlgFe as an adsorbent is notable, and it can be established that it is highly effective for removing As(V).

Thermodynamic parameters

Thermodynamic parameters, like the change in enthalpy ($\Delta H°$) and the change in entropy ($\Delta S°$), were calculated to establish the adsorption process feasibility and the temperature effect on both adsorbate-microspheres systems. These parameters were calculated by mathematical equations reported in the literature (Khalid *et al.* 2005), using As(V) concentrations before and after adsorption equilibrium for both adsorbate-adsorbent systems. Values of $\Delta H° = 6{,}973.5337$ J/mol y $\Delta S° = -32.4686$ J/mol K were obtained for AlgN, and $\Delta H° = 26{,}231.5014$ J/mol y $\Delta S° = 34.7641$ J/mol K for AlgFe. Experimental data were also fitted to the Dubinin-Radushkevich isotherm model (D-R) to determine if the ion-exchange process significantly affects the sorption mechanism (Sarkar *et al.* 2006). This isotherm model also assumes a heterogeneous nature of the sorption process (equation S2) (Bering *et al.* 1972):

Table 4 | Maximum adsorption capacities for As(V) ions of various adsorbents

Adsorbent	Q (mg/g)	pH	Temperature (°C)	Reference
AlgN	0.9895	6	25	This work
AlgFe	1.2173	6	25	This work
Iron-oxide modified sericite alginate beads	21.61	4.5	25	Lalhmunsiama *et al.* (2017)
Magnetic nanoparticles impregnated chitosan beads	35.7	6.8	~25	Wang *et al.* (2014b)
Alginate beads containing Fe and Mn oxides	0.78	7	~25	Ociński *et al.* (2016)
Activated carbon-supported nano-TiO_2	15.18	8	~25	Luo *et al.* (2020)
Iron treated biochar	6.77	6	25	Tan *et al.* (2020)
Magnetic xerogel monoliths	0.0628	5	25	Khamkure *et al.* (2021)
Iron-modified sorghum straw biochar	23	5	~25	Zang *et al.* (2021)
Iron oxide nanoparticle functionalized activated carbon	32.57	2–5	25	Ha *et al.* (2021)

The linear form of the D-R isotherm is (Argun *et al.* 2007):

$$\mathrm{Ln}\, q_e = \ln X_m - K\varepsilon^2 \tag{4}$$

The slopes and intercepts values obtained from the graphs of Ln q_e vs. ε^2 graphs for both arsenate-microspheres systems (not shown) were used to calculate X_m and K. The sorption energy, which is the energy change necessary for the transfer of one mole of arsenate to the solid's surface, was determined using K value, as follows (Atun & Kilislioglu 2003):

$$\Delta G^0 = -E = (-2K)^{-1/2} \tag{5}$$

$\Delta G°$ value may be associated with the reaction mechanism. If the $8 < \Delta G° < 16$ kJ/mol, ion exchange is the system's primary sorption mechanism. If $\Delta G° < 8$ kJ/mol, physisorption is the primary mechanism (Atun & Kilislioglu 2003). As shown in Table S1, the adsorption energies (ΔG^0) are higher than 8 kJ/mol for all cases, except at 25 °C for the AlgN system, where the $\Delta G°$ value is close to 8. This fact can be taken as evidence that chemisorption controlled all studied systems and that these mechanisms are essential for diffusion and efficiency in such systems (Argun *et al.* 2007).

As mentioned above, these parameters demonstrate that the adsorption process is endothermic. This result supports the conclusion that as temperature rises, the adsorption capacities of AlgN and AlgFe for As(V) increase. Furthermore, since the $\Delta S°$ values were positive for AlgFe, the rise in entropy change is a consequence of adsorption. Redistribution of energy in the arsenate-adsorbent systems is responsible for this behavior. Arsenate ions close to the microspheres' surface are more ordered before adsorption, and a higher proportion of free arsenic ions against those close to the adsorbent's surface will occur if such ratio is compared to the adsorbed ions. Consequently, the interaction may become a reversible process that favors the materials' regeneration. For both AlgN and AlgFe systems, adsorption will take place at high and medium temperatures since $\Delta H° > 0$; however, for AlgN $\Delta S° < 0$, the adsorbate-adsorbent interaction could thus present low reversibility (Argun *et al.* 2007).

CONCLUSIONS

According to the results obtained in this work, the natural alginate microspheres (AlgN) have a relatively high As(V) adsorption capacity; this capacity increases when subjected to iron nanoparticles' encapsulation (AlgFe). Both adsorbents presented a significantly high adsorption kinetic rate due to the small particle size and to the surface modification with FeNPs. FeNPs were successfully encapsulated and uniformly disseminated over the surface of the microspheres using a simple and low FeNPs concentration approach. A chemisorption mechanism was identified in both adsorbate-adsorbent systems. Different functional groups removed As(V), indicating heterogeneous adsorption and denoting actives sites with different adsorption energies. The solution pH plays an essential role in As(V) adsorption since the removal increases at slightly acidic pH values. An endothermic process controls the removal of As(V) in both materials. Moreover, when using AlgFe, the process can be more reversible than when using AlgN, which indicates that the modification of the alginate with FeNPs is favorable for the regeneration of the adsorbent and higher efficiency of As(V) removal.

ACKNOWLEDGEMENTS

Authors acknowledge technical support by S.A. Valencia-Leal, and financial support by Coordinación de la Investigación Científica-UMSNH (grant: CIC-UMSNH-2021).

DATA AVAILABILITY STATEMENT

All relevant data are included in the paper or its Supplementary Information.

REFERENCES

Alp Arıcı, T., Özcan, A. S. & Özcan, A. 2020 Biosorption characteristics of Cu(II) and Cd(II) ions by modified alginate. *Journal of Polymers and the Environment* **28**, 3221–3234. https://doi.org/10.1007/s10924-020-01844-2.

Argun, M. E., Dursun, S., Ozdemir, C. & Karatas, M. 2007 Heavy metal adsorption by modified oak sawdust: thermodynamics and kinetics. *Journal of Hazardous Materials* **141**, 77–85. https://doi.org/10.1016/j.jhazmat.2006.06.095.

Atun, G. & Kilislioglu, A. 2003 Adsorption behavior of cesium on montmorillonite-type clay in the presence of potassium ions. *Journal of Radioanalytical and Nuclear Chemistry* **258**, 605–611. https://doi.org/10.1023/B:JRNC.0000011757.59069.ba.

Ayoob, S., Gupta, A. K., Bhakat, P. B. & Bhat, V. T. 2008 Investigations on the kinetics and mechanisms of sorptive removal of fluoride from water using alumina cement granules. *Chemical Engineering Journal* **140**, 6–14. https://doi.org/10.1016/j.cej.2007.08.029.

Benyoucef, S. & Amrani, M. 2011 Removal of phosphorus from aqueous solutions using chemically modified sawdust of Aleppo pine (*Pinus halepensis Miller*): kinetics and isotherm studies. *Environmentalist* **31**, 200–207. https://doi.org/10.1007/s10669-011-9313-1.

Bering, B. P., Dubinin, M. M. & Serpinsky, V. V. 1972 On thermodynamics of adsorption in micropores. *Journal of Colloid and Interface Science* **38**, 185–194. https://doi.org/10.1016/0021-9797(72)90233-0.

Bezbaruah, A. N., Kalita, H., Almeelbi, T., Capecchi, C. L., Jacob, D. L., Ugrinov, A. G. & Payne, S. A. 2014 Ca–alginate-entrapped nanoscale iron: arsenic treatability and mechanism studies. *Journal of Nanoparticle Research* **16**, 2175. https://doi.org/10.1007/s11051-013-2175-3.

Boffetta, P., Zunarelli, C. & Borron, C. 2020 Dose-response analysis of exposure to arsenic in drinking water and risk of skin lesions: a systematic review of the literature. *Dose-Response* **18**, 1559325820957823. https://doi.org/10.1177/1559325820957823.

Burillo, J. C., Ballinas, L., Burillo, G., Guerrero-Lestarjette, E., Lardizabal-Gutierrez, D. & Silva-Hidalgo, H. 2021 Chitosan hydrogel synthesis to remove arsenic and fluoride ions from groundwater. *Journal of Hazardous Materials* **417**, 126070. https://doi.org/10.1016/j.jhazmat.2021.126070.

Chowdhury, S., Chowdhury, I. R., Kabir, F., Mazumder, M. A. J., Zahir, M. H. & Alhooshani, K. 2019 Alginate-based biotechnology: a review on the arsenic removal technologies and future possibilities. *Journal of Water Supply: Research and Technology-Aqua* **68**, 369–389. https://doi.org/10.2166/aqua.2019.005.

Daemi, H. & Barikani, M. 2012 Synthesis and characterization of calcium alginate nanoparticles, sodium homopolymannuronate salt and its calcium nanoparticles. *Scientia Iranica* **19**, 2023–2028. https://doi.org/10.1016/j.scient.2012.10.005.

Dayananda, D., Sarva, V. R., Prasad, S. V., Arunachalam, J. & Ghosh, N. N. 2014 Preparation of CaO loaded mesoporous Al_2O_3: efficient adsorbent for fluoride removal from water. *Chemical Engineering Journal* **248**, 430–439. https://doi.org/10.1016/j.cej.2014.03.064.

Dutta, M., Ray, T. & Basu, J. K. 2012 Batch adsorption of fluoride ions onto microwave assisted activated carbon derived from *Acacia Auriculiformis* scrap wood. *Archives of Applied Science Research* **4**, 536–550.

Flores-Garay, K. A., Martínez-Luévanos, A., Cruz-Ortiz, B. R., García-Cerda, L. A. & López-Badillo, C. M. 2016 Síntesis de silicatos de calcio por el método Pechini e intercambio iónico de alginato de sodio-cloruro de calcio. *Boletín de la Sociedad Española de Cerámica y Vidrio* **55**, 239–245. https://doi.org/10.1016/j.bsecv.2016.05.002.

Geethamani, C. K., Ramesh, S. T., Gandhimathi, R. & Nidheesh, P. V. 2013 Fluoride sorption by treated fly ash: kinetic and isotherm studies. *Journal of Material Cycles and Waste Management* **15**, 381–392. https://doi.org/10.1007/s10163-013-0128-7.

Ghani, M., Rezaei, B., Aghaji, A. G. & Arami, M. 2016 Novel cross-linked superfine alginate-based nanofibers: fabrication, characterization, and their use in the adsorption of cationic and anionic dyes. *Advances in Polymer Technology* **35**, 428–438. https://doi.org/10.1002/adv.21569.

Giles, C. H., D'Silva, A. P. & Easton, I. A. 1974a A general treatment and classification of the solute adsorption isotherm part. II. Experimental interpretation. *Journal of Colloid and Interface Science* **47**, 766–778. https://doi.org/10.1016/0021-9797(74)90253-7.

Giles, C. H., Smith, D. & Huitson, A. 1974b A general treatment and classification of the solute adsorption isotherm. I. theoretical. *Journal of Colloid and Interface Science* **47**, 755–765. https://doi.org/10.1016/0021-9797(74)90252-5.

Gong, R., Ding, Y., Liu, H., Chen, Q. & Liu, Z. 2005 Lead biosorption and desorption by intact and pretreated spirulina maxima biomass. *Chemosphere* **58**, 125–130. https://doi.org/10.1016/j.chemosphere.2004.08.055.

Guo, L., Du, Y., Yi, Q., Li, D., Cao, L. & Du, D. 2015 Efficient removal of arsenic from 'dirty acid' wastewater by using a novel immersed multi-start distributor for sulphide feeding. *Separation and Purification Technology* **142**, 209–214. https://doi.org/10.1016/j.seppur.2014.12.029.

Ha, H. T., Phong, P. T. & Minh, T. D. 2021 Synthesis of iron oxide nanoparticle functionalized activated carbon and its applications in arsenic adsorption. *Journal of Analytical Methods in Chemistry* **2021**, e6668490. https://doi.org/10.1155/2021/6668490.

Habuda-Stanić, M. & Nujić, M. 2015 Arsenic removal by nanoparticles: a review. *Environmental Science & Pollution Research* **22**, 8094–8123. https://doi.org/10.1007/s11356-015-4307-z.

Hassan, A. F., Abdel-Mohsen, A. M. & Elhadidy, H. 2014 Adsorption of arsenic by activated carbon, calcium alginate and their composite beads. *International Journal of Biological Macromolecules* **68**, 125–130. https://doi.org/10.1016/j.ijbiomac.2014.04.006.

Hernández Ordáz, G., Segura Castruita, M. A., Álvarez González Pico, L. C., Aldaco Nuncio, R. A., Fortis Hernández, M., González Cervantes, G., Hernández Ordáz, G., Segura Castruita, M. A., Álvarez González Pico, L. C., Aldaco Nuncio, R. A., Fortis Hernández, M. & González Cervantes, G. 2013 Comportamiento del arsénico en suelos de la región lagunera de Coahuila, México. *Terra Latinoamericana* **31**, 295–303.

Ho, Y. S. & McKay, G. 2002 Application of kinetic models to the sorption of Copper(II) on to peat. *Adsorption Science & Technology* **20**, 797–815. https://doi.org/10.1260/026361702321104282.

Ho, Y. S., McKay, G., Wase, D. A. J. & Forster, C. F. 2000 Study of the sorption of divalent metal ions on to peat. *Adsorption Science & Technology* **18**, 639–650. https://doi.org/10.1260/0263617001493693.

Khalid, N., Rahman, S. & Ahmad, S. 2005 Potential of sawdust for the decontamination of lead from aqueous media. *Separation Science and Technology* **40**, 2427–2443. https://doi.org/10.1080/01496390500267467.

Khamkure, S., Garrido-Hoyos, S. E., Gamero-Melo, P. & Reyes-Rosas, A. 2021 Synthesis and characterization of magnetic xerogel monolith as an adsorbent for As(V) removal from groundwater. *Processes* **9**, 386. https://doi.org/10.3390/pr9020386.

Kumar, R., Patel, M., Singh, P., Bundschuh, J., Pittman, C. U., Trakal, L. & Mohan, D. 2019 Emerging technologies for arsenic removal from drinking water in rural and peri-urban areas: methods, experience from, and options for Latin America. *Science of The Total Environment* **694**, 133427. https://doi.org/10.1016/j.scitotenv.2019.07.233.

Kumar, M., Goswami, R., Patel, A. K., Srivastava, M. & Das, N. 2020 Scenario, perspectives and mechanism of arsenic and fluoride Co-occurrence in the groundwater: a review. *Chemosphere* **249**, 126126. https://doi.org/10.1016/j.chemosphere.2020.126126.

Lagergren, S. 1898 Zur theorie der sogenannten adsorption gelosterstoffe. Kungliga svenska vetenskapsakademiens. *Handlingar* **24**, 1–39.

Lalhmunsiama Pawar, R. R., Hong, S.-M., Jin, K. J. & Lee, S.-M. 2017 Iron-oxide modified sericite alginate beads: a sustainable adsorbent for the removal of As(V) and Pb(II) from aqueous solutions. *Journal of Molecular Liquids* **240**, 497–503. https://doi.org/10.1016/j.molliq.2017.05.086.

Lavanya, K. M., Florence, J. A. K., Vivekanandan, B. & Lakshmipathy, R. 2021 Comparative investigations of raw and alkali metal free banana peel as adsorbent for the removal of Hg^{2+} ions. *Materials Today: Proceedings*. https://doi.org/10.1016/j.matpr.2021.07.410

Lim, S.-F., Zheng, Y.-M., Zou, S.-W. & Chen, J. P. 2009 Uptake of arsenate by an alginate-encapsulated magnetic sorbent: process performance and characterization of adsorption chemistry. *Journal of Colloid and Interface Science* **333**, 33–39. https://doi.org/10.1016/j.jcis.2009.01.009.

Low, M. J. D. 1960 Kinetics of chemisorption of gases on solids. *Chemical Reviews* **60** (3), 267–312. https://doi.org/10.1021/cr60205a003.

Luo, Q., Li, G., Chen, M., Qin, F., Li, H. & Qiang, Y. 2020 Effect factor of arsenite and arsenate removal by a manufactured material: activated carbon-supported nano-TiO_2. *Journal of Chemistry* **2020**, e6724157. https://doi.org/10.1155/2020/6724157.

Lv, X., Jiang, G., Xue, X., Wu, D., Sheng, T., Sun, C. & Xu, X. 2013 Fe0-Fe_3O_4 nanocomposites embedded polyvinyl alcohol/sodium alginate beads for chromium (VI) removal. *Journal of Hazardous Materials* **262**, 748–758. https://doi.org/10.1016/j.jhazmat.2013.09.036.

Maity, J. P., Vithanage, M., Kumar, M., Ghosh, A., Mohan, D., Ahmad, A. & Bhattacharya, P. 2021 Seven 21st century challenges of arsenic-fluoride contamination and remediation. *Groundwater for Sustainable Development* **12**, 100538. https://doi.org/10.1016/j.gsd.2020.100538.

Mandal, S., Sahu, M. K. & Patel, R. K. 2013 Adsorption studies of arsenic(III) removal from water by zirconium polyacrylamide hybrid material (ZrPACM-43). *Water Resources and Industry* **4**, 51–67. https://doi.org/10.1016/j.wri.2013.09.003.

Nazari, M. & Halladj, R. 2014 Adsorptive removal of fluoride ions from aqueous solution by using sonochemically synthesized nanomagnesia/alumina adsorbents: an experimental and modeling study. *Journal of the Taiwan Institute of Chemical Engineers* **45**, 2518–2525. https://doi.org/10.1016/j.jtice.2014.05.020.

Ociński, D., Jacukowicz-Sobala, I. & Kociołek-Balawejder, E. 2016 Alginate beads containing water treatment residuals for arsenic removal from water – formation and adsorption studies. *Environmental Science & Pollution Research* **23**, 24527–24539. https://doi.org/10.1007/s11356-016-6768-0.

Osuna-Martínez, C. C., Armienta, M. A., Bergés-Tiznado, M. E. & Páez-Osuna, F. 2021 Arsenic in waters, soils, sediments, and biota from Mexico: an environmental review. *Science of The Total Environment* **752**, 142062. https://doi.org/10.1016/j.scitotenv.2020.142062.

Palma-Lara, I., Martínez-Castillo, M., Quintana-Pérez, J. C., Arellano-Mendoza, M. G., Tamay-Cach, F., Valenzuela-Limón, O. L., García-Montalvo, E. A. & Hernández-Zavala, A. 2020 Arsenic exposure: a public health problem leading to several cancers. *Regulatory Toxicology and Pharmacology* **110**, 104539. https://doi.org/10.1016/j.yrtph.2019.104539.

Papageorgiou, S. K., Kouvelos, E. P. & Katsaros, F. K. 2008 Calcium alginate beads from *Laminaria digitata* for the removal of Cu^{+2} and Cd^{+2} from dilute aqueous metal solutions. *Desalination* **224** (1–3), 293–306. https://doi.org/10.1016/j.desal.2007.06.011.

Ramos-Vargas, S., Alfaro-Cuevas-Villanueva, R., Huirache-Acuña, R. & Cortés-Martínez, R. 2018 Removal of fluoride and arsenate from aqueous solutions by aluminum-modified guava seeds. *Applied Sciences* **8**, 1807. https://doi.org/10.3390/app8101807.

Safarik, I. & Safarikova, M. 2013 One-step magnetic modification of non-magnetic solid materials. *International Journal of Materials Research* **105** (1), 104–107. https://doi.org/10.3139/146.111009.

Santos, T. R. T., Silva, M. F., Nishi, L., Vieira, A. M. S., Klein, M. R. F., Andrade, M. B., Vieira, M. F. & Bergamasco, R. 2016 Development of a magnetic coagulant based on *Moringa oleifera* seed extract for water treatment. *Environmental Science & Pollution Research* **23**, 7692–7700. https://doi.org/10.1007/s11356-015-6029-7.

Sarkar, M., Banerjee, A. & Pramanick, P. P. 2006 Kinetics and mechanism of fluoride removal using laterite. *Industrial & Engineering Chemistry Research* **45**, 5920–5927. https://doi.org/10.1021/ie060016j.

Sigdel, A., Lim, J., Park, J., Kwak, H., Min, S., Kim, K., Lee, H., Nahm, C. H. & Park, P.-K. 2018 Immobilization of hydrous iron oxides in porous alginate beads for arsenic removal from water. *Environmental Science: Water Research & Technology* **4** (8), 1114–1123. https://doi.org/10.1039/C8EW00084 K.

Sousa, F. L., Daniel-da-Silva, A. L., Silva, N. J. O. & Trindade, T. 2015 Bionanocomposites for magnetic removal of water pollutants. In: *Eco-Friendly Polymer Nanocomposites: Chemistry and Applications, Advanced Structured Materials* (Thakur, V. K. & Thakur, M. K., eds). Springer India, New Delhi, pp. 279–310. https://doi.org/10.1007/978-81-322-2473-0_9

Swain, S. K., Patnaik, T., Patnaik, P. C., Jha, U. & Dey, R. K. 2013 Development of new alginate entrapped Fe(III)–Zr(IV) binary mixed oxide for removal of fluoride from water bodies. *Chemical Engineering Journal* **215–216**, 763–771. https://doi.org/10.1016/j.cej.2012.10.098.

Tan, G., Mao, Y., Wang, H. & Xu, N. 2020 A comparative study of arsenic(V), tetracycline and nitrate ions adsorption onto magnetic biochars and activated carbon. *Chemical Engineering Research and Design* **159**, 582–591. https://doi.org/10.1016/j.cherd.2020.05.011.

Thomas-Busan, C., Andrei Sarabia-Sainz, J., García-Hernández, J., Madera-Santana, T., Vázquez-Moreno, L. & Montfort, G. R.-C. 2020 Synthesis of alginate–polycation capsules of different composition: characterization and their adsorption for [As(III)] and [As(V)] from aqueous solutions. *RSC Advances* **10**, 28755–28765. https://doi.org/10.1039/D0RA05135G.

Valenzuela, C., Hernández, V., Morales, M. S., Neira-Carrillo, A. & Pizarro, F. 2014 Preparation and characterization of heme iron-alginate beads. *LWT-Food Science and Technology* **59** (2), 1283–1289. https://doi.org/10.1016/j.lwt.2014.04.030.

Wang, T., Jin, X., Chen, Z., Megharaj, M. & Naidu, R. 2014a Green synthesis of Fe nanoparticles using eucalyptus leaf extracts for treatment of eutrophic wastewater. *Science of The Total Environment* **466–467**, 210–213. https://doi.org/10.1016/j.scitotenv.2013.07.022.

Wang, J., Xu, W., Chen, L., Huang, X. & Liu, J. 2014b Preparation and evaluation of magnetic nanoparticles impregnated chitosan beads for arsenic removal from water. *Chemical Engineering Journal* **251**, 25–34. https://doi.org/10.1016/j.cej.2014.04.061.

Wang, P., Ma, Q., Hu, D. & Wang, L. 2015 Removal of Reactive Blue 21 onto magnetic chitosan microparticles functionalized with polyamidoamine dendrimers. *Reactive and Functional Polymers* **91–92**, 43–50. https://doi.org/10.1016/j.reactfunctpolym.2015.04.007.

Wang, A., Zhou, K., Zhang, X., Zhou, D., Peng, C. & Chen, W. 2020 Arsenic removal from highly-acidic wastewater with high arsenic content by copper-chloride synergistic reduction. *Chemosphere* **238**, 124675. https://doi.org/10.1016/j.chemosphere.2019.124675.

Wei, Y.-T., Zheng, Y.-M. & Chen, J. P. 2011 Uptake of methylated arsenic by a polymeric adsorbent: process performance and adsorption chemistry. *Water Research* **45**, 2290–2296. https://doi.org/10.1016/j.watres.2011.01.002.

Xi, Z. & Chen, B. 2014 Removal of polycyclic aromatic hydrocarbons from aqueous solution by raw and modified plant residue materials as biosorbents. *Journal of Environmental Sciences* **26**, 737–748. https://doi.org/10.1016/S1001-0742(13)60501-X.

Xiang, W., Zhang, G., Zhang, Y., Tang, D. & Wang, J. 2014 Synthesis and characterization of cotton-like Ca–Al–La composite as an adsorbent for fluoride removal. *Chemical Engineering Journal* **250**, 423–430. https://doi.org/10.1016/j.cej.2014.03.118.

Ye, Z., Meng, Q. & Lu, S. 2012 Adsorption of 2,4,6-trinitrotoluene on carboxylated porous polystyrene microspheres. *Applied Surface Science* **258**, 3624–3628. https://doi.org/10.1016/j.apsusc.2011.11.126.

Zang, S., Zuo, Y., Wang, J., Liu, X., Gomez, M. A. & Wei, L. 2021 Adsorption removal of roxarsone, arsenite(III), and arsenate(V) using iron-modified sorghum straw biochar and its kinetics. *Acta Geochimica* **40**, 409–418. https://doi.org/10.1007/s11631-021-00466-2.

First received 6 September 2021; accepted in revised form 24 November 2021. Available online 9 December 2021